ACSNANO
www.acsnano.org
ARTICLE

Two-Orbital Kondo Screening in a Self-Assembled Metal–Organic Complex

Giulia E. Pacchioni, Marina Pivetta, Luca Gragnaniello, Fabio Donati, Gabriel Autès, Oleg V. Yazyev, Stefano Rusponi, and Harald Brune*

Institute of Physics, Ecole Polytechnique Fédérale de Lausanne (EPFL), CH-1015 Lausanne, Switzerland

Supporting Information

ABSTRACT: **Iron atoms adsorbed on a Cu(111) surface and buried under polyphenyl dicarbonitrile molecules exhibit strongly spatial anisotropic Kondo features with directionally dependent Kondo temperatures and line shapes, as evidenced by scanning tunneling spectroscopy. First-principles calculations find nearly full polarization for the half-filled Fe $3d_{xz}$ and $3d_{yz}$ orbitals, which therefore can give rise to Kondo screening with the experimentally observed directional dependence and distinct Kondo temperatures. X-ray absorption spectroscopy and X-ray magnetic circular dichroism measurements confirm that the spin in both channels is effectively Kondo-screened. At ideal Fe coverage, these two-orbital Kondo impurities are arranged in a self-assembled honeycomb superlattice.**

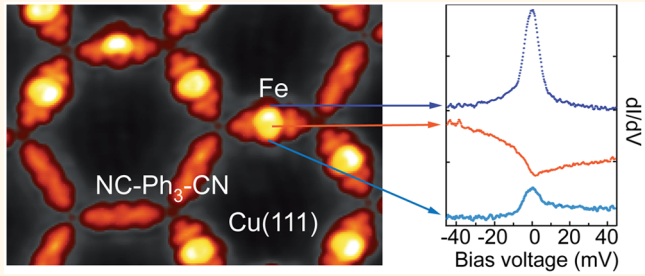

KEYWORDS: *Kondo effect, organometallic complex, self-assembly, scanning tunneling spectroscopy, X-ray absorption spectroscopy, X-ray magnetic circular dichroism, density functional theory*

The interaction between a magnetic impurity and the conduction electrons of a nonmagnetic host can give rise to a many-body singlet state manifesting itself as a sharp resonance near the Fermi energy (E_F). This is known as Kondo effect[1] and was originally observed in bulk solids containing magnetic impurities. Subsequently, it has been reported for various low-dimensional systems, such as surface-adsorbed magnetic atoms[2−4] and semiconductor quantum dots.[5,6] In recent years, great attention was devoted also to organic and metal−organic molecules, owing to their potential for single-molecule spintronic applications.[7,8] Moreover, the Kondo effect in molecular systems can be manipulated in a controlled way. In particular, it can be turned on and off by adsorbing atoms or small molecules,[9−13] by detaching peripheral hydrogen atoms,[14] by supramolecular interactions,[15,16] or by modifying the molecular conformation with voltage pulses.[17−19] The study of more complex Kondo systems, for example, those with more than one available screening channel, can give further insight into Kondo physics and possibly lead to different tools for the control of magnetism and spintronics at the nanoscale. To date, however, molecular systems in which more than one orbital can contribute to Kondo screening have rarely been investigated.[20−23]

Here, we report on a Kondo effect with two orbital contributions, each of them having distinct Kondo temperature and location, as evidenced by scanning tunneling spectroscopy (STS) measurements. We obtain this system by the combination of magnetic atoms with purely organic molecules; namely, we adsorb Fe atoms under NC-Ph_3-CN molecules in $(NC\text{-}Ph_3\text{-}CN)_3Cu_2$ networks on Cu(111). The Kondo effect arises from the presence of two singly occupied Fe d orbitals with different spatial distribution and hybridization with the molecular orbitals, as evidenced by density functional theory (DFT) calculations. The spatial distribution of the Kondo features reflects the anisotropy of the Fe-molecule hybridization. X-ray magnetic circular dichroism (XMCD) reveals that the spin in both Kondo channels is fully screened. Adjusting the Fe coverage, we obtain samples where exactly one Fe atom is buried under one NC-Ph_3-CN molecule and thus create an ordered superlattice of two-orbital Kondo species. Moreover, we discuss the results obtained replacing Fe with Co, known to be a Kondo impurity when adsorbed on Cu(111). In the metal−organic complex, its Kondo signature disappears, coherently with the d orbital occupation obtained from our DFT calculations.

RESULTS AND DISCUSSION

Deposition of NC-Ph_3-CN polyphenyl molecules[24] on the Cu(111) substrate at 300 K yields a $(NC\text{-}Ph_3\text{-}CN)_3Cu_2$ honeycomb network.[25] Subsequent Fe deposition at 10 ± 2 K leads to the coexistence of three Fe-related species, as demonstrated by the scanning tunneling microscopy (STM) image of Figure 1a. Atoms landing in the hexagonal cavities

Received: November 4, 2016
Accepted: February 24, 2017
Published: February 24, 2017

DOI: 10.1021/acsnano.6b07431
ACS Nano 2017, 11, 2675−2681

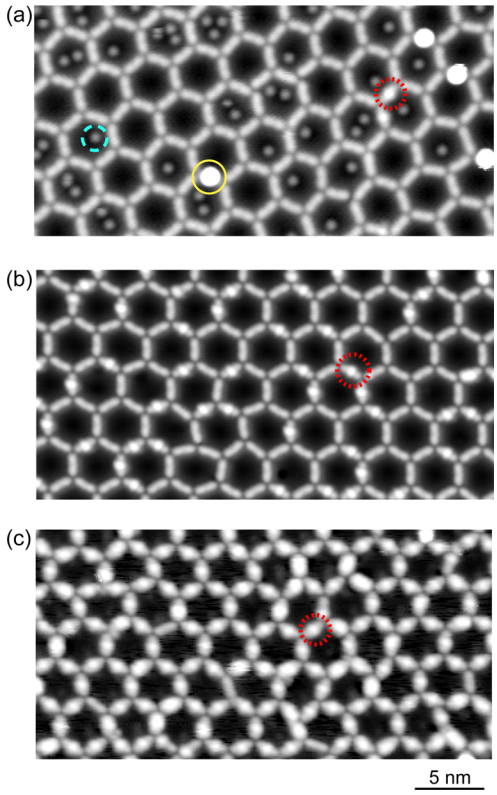

Figure 1. (a) $(NC\text{-}Ph_3\text{-}CN)_3Cu_2$ honeycomb network on Cu(111) with $\Theta = (6 \pm 1) \times 10^{-3}$ monolayers (ML) of Fe, $T_{dep} = 10 \pm 2$ K ($V_t = -200$ mV, $I_t = 100$ pA, $T_{STM} = 5$ K). Dashed turquoise circle, Fe atom/Cu(111); solid yellow circle, Fe atom on top of molecule; dotted red circle, Fe atom under molecule. (b) Fe deposition at $T_{dep} = 20 \pm 2$ K ($\Theta = (6 \pm 1) \times 10^{-3}$ ML, $V_t = -50$ mV, $I_t = 300$ pA, $T_{STM} = 5$ K). (c) Deposition of $\Theta = (18 \pm 1) \times 10^{-3}$ ML of Fe at $T_{dep} = 50 \pm 2$ K ($V_t = -500$ mV, $I_t = 100$ pA, $T_{STM} = 50$ K).

stick on their site of impact without thermal diffusion toward the molecules, similar to what has been observed for Fe deposition on $(NC\text{-}Ph_5\text{-}CN)_3Cu_2/Cu(111)$ networks.[26] The Fe atoms appear as well localized protrusions (turquoise dashed circle). On the organic ligands, two Fe-related features are discerned by their apparent height. The very bright features (yellow full circle) readily disappear through repeated STM imaging (see Supporting Information). We systematically observe after such an event that empty cavities in the immediate vicinity of the displaced element become occupied by a single Fe atom. Thus, the bright protrusions are identified as Fe atoms adsorbed onto the organic molecules. In contrast, the less bright features (red dotted circle) are very robust against manipulation with the STM tip and attributed to Fe atoms below the organic molecules.

When Fe is deposited at higher temperature (18 K < T_{dep} < 50 K), Fe diffusion within the cavities and down from the molecules is activated, and all atoms are found under the molecules (Figure 1b,c). From these observations, we infer that the buried adsorption site is the most stable one, whereas the other two are metastable.[27] In Figure 1c, the Fe coverage corresponds to one Fe atom per molecule: in most cases, there is exactly one Fe atom below one molecule, and there are only few molecules that have no or two Fe atoms underneath. Therefore, we are able to create a regular lattice of buried Fe atoms.

The electronic structure of Fe atoms adsorbed on the substrate and under the molecules has been characterized by means of STS. The differential conductance spectra (dI/dV) acquired on Fe/Cu(111) (see Figure 2a) show no noteworthy

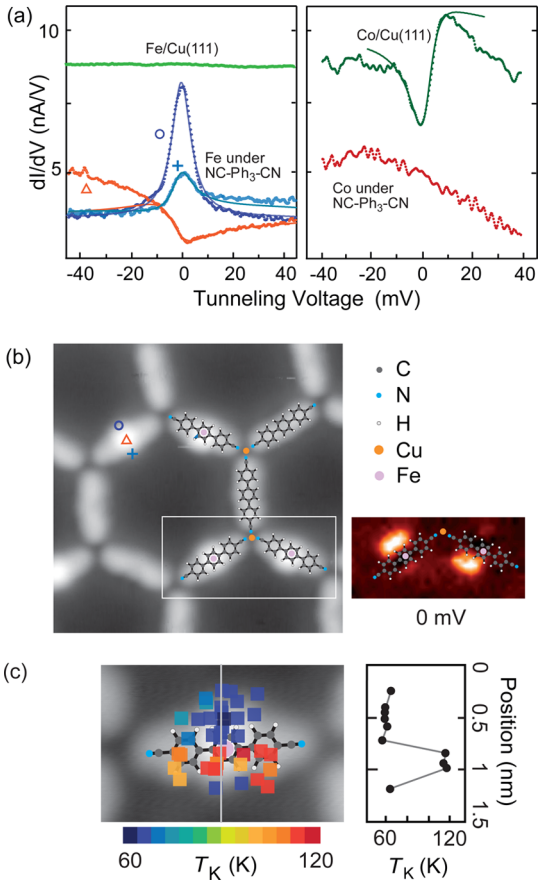

Figure 2. (a) Left: dI/dV spectra acquired on an Fe atom on Cu(111) (green) and on an Fe atom buried by NC-Ph_3-CN at the three locations indicated in (b) by the corresponding symbols. Solid lines are fits by eq 1 (spectroscopy parameters: $V_t = -50$ mV, $I_t = 300$ pA, $V_{mod} = 2$ mV at 523 Hz). Right: dI/dV spectra on a Co atom on Cu(111) (green) and under a molecule (red). Solid line is a fit by eq 1 (spectroscopy parameters: $V_t = -50$ mV, $I_t = 50$ pA, $V_{mod} = 2$ mV at 523 Hz). (b) Left: STM image showing bare molecules and molecules burying Fe atoms; part of the honeycomb lattice is reproduced by the overlaid model. The locations of the point spectra of (a) are indicated. The white rectangle highlights the region corresponding to the dI/dV map at E_F shown on the right. (c) Left: Map of T_K deduced from point spectra acquired on a molecule burying an Fe atom. Right: Variation of T_K along the indicated gray line.

spectral features around E_F, similar to the spectra acquired on undecorated molecules and on Fe atoms on top of molecules reported in the Supporting Information. In contrast, spectra acquired on molecules covering an Fe adatom show large variations of the differential conductance close to E_F, with a marked spatial variation across the molecule; see the symbols in Figure 2b for the location of the spectra. The conductance exhibits an intense peak on one side (○), a dip above the molecule (△), and a smaller peak on the other side of the molecule (+).

The spatial distribution of the two types of resonances can be seen in more detail in the dI/dV map shown together with the

DOI: 10.1021/acsnano.6b07431
ACS Nano 2017, 11, 2675−2681

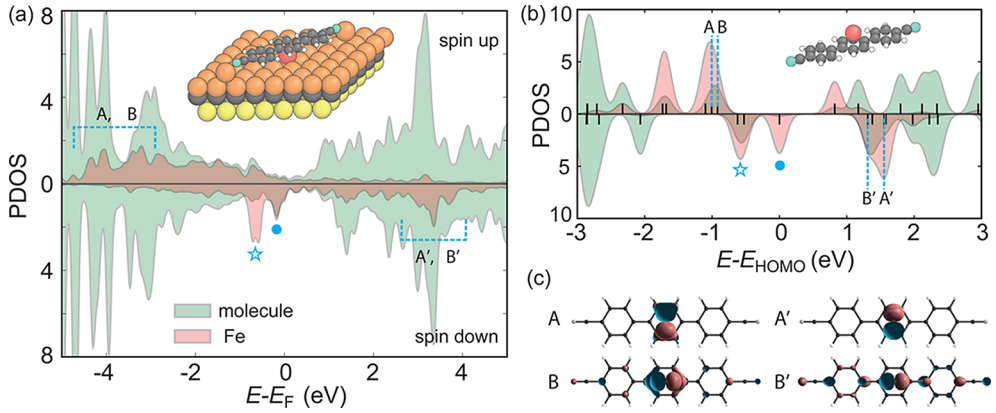

Figure 3. (a) Spin-resolved projected density of states (PDOS) of the surface-supported system, showing the projections on the Fe atom (red) and on the molecule (green). Inset: Slab geometry after relaxation. (b) Same as (a) but for the free-standing Fe-molecule system. (c) Density isosurface (0.002 e^{-}/a_0^3) of the free-standing Fe-molecule system wave functions corresponding to A, B, A′, and B′; blue and red indicate the orbital phase.

constant current image in Figure 2b. The image shows the NC-Ph_3-CN in the honeycomb network, with some molecules presenting an Fe atom below the central phenyl ring. The dI/dV map was acquired on the region highlighted by the white rectangle, thus comprising two molecules burying Fe atoms. A large bright spot is visible on one side of each molecule and a smaller, less bright one on the respective other side. For each molecule, a darker region is detected between the bright spots. Comparison with the spectra shown in Figure 2a reveals that the brightest and largest spot in the dI/dV map corresponds to the intense peak (○). The dip (△) appears as a depression in the map, whereas the peak with smaller amplitude (+) is related to the less bright and smaller feature on the other side of each molecule. The higher intensity observed on one side of the molecules is ascribed to the tilt of the phenyl rings with respect to the surface and to each other.[25,28,29] Notice that very similar results have been obtained for Fe atoms buried by NC-Ph_5-CN molecules (see Supporting Information).

We attribute these different spectral features to a manifestation of spatially varying Kondo screening. To substantiate this interpretation, we fit the spectra with a Fano function[30]

$$\Phi(E) = \frac{(q\Gamma + E - E_0)^2}{\Gamma^2 + (E - E_0)^2} \quad (1)$$

with E_0 being the energy position of the resonance and Γ its half-width at half-maximum; q determines the line shape of the curve. Γ has a characteristic dependence on temperature expressed by $2\Gamma = [(\alpha k_B T)^2 + (2\Gamma_0)^2]^{1/2}$.[31,32] Γ_0, the half-width at 0 K, is related to the Kondo temperature T_K by $\Gamma_0 = k_B T_K$. The fit with eq 1 agrees very well with experiment in the relevant energy interval around E_F (see Figure 2a). The peaks on both sides of the molecule yield consistent Kondo temperatures of $T_K = 63 \pm 4$ and 62 ± 3 K, whereas the dip gives a significantly higher value of $T_K = 114 \pm 5$ K (see Supporting Information for the fitting parameters). From these results, we deduce that the Kondo features left and right of the molecular axis belong to one class and the one on the axis to another.

The spatial distribution of the Kondo temperature is shown in Figure 2c. The map was derived from fitting with eq 1 a set of point spectra acquired across the molecule. It shows two distinct T_K values with a sharp transition from one to the other, as evidenced by the profile taken perpendicular to the molecular axis and through the center of the molecule, indicated by the gray line. The bright areas seen on the dI/dV map at E_F (Figure 2b) display the lower T_K value and the peak-like line shape, whereas along the molecular axis, T_K doubles and the Kondo effect leads to a dip. Therefore, there is a correlation between line shape and width: peaks correspond to lower T_K and dips to higher T_K. Spatial variations of T_K were reported for TBrPP-Co molecules on Cu(111)[33] and for Fe(II) P on Au(111).[23] These systems displayed a smooth increase of T_K from the center to the periphery of the molecule, that is, over a distance greater than 0.3 nm. Moreover, no significant changes in the line shape were observed, with all spectra showing a dip. In contrast, our system shows a sharp transition within a distance of 0.1 nm, without intermediate values of T_K. This abrupt transition between the two T_K values and line shapes hints toward the coexistence of two Kondo channels with different coupling to the conduction electrons of the substrate.

To gain more insight into the Kondo effect observed upon formation of the metal−organic complex, we replaced Fe with Co. As for Fe, Co atoms, three possible adsorption positions for $T_{dep} = 10$ K are present: on the substrate, on top of molecules, and under molecules. Co is known to be a Kondo impurity on the bare Cu(111) substrate,[3,34] and our STS measurements, shown in Figure 2a, reproduce the reported Fano dip with $T_K = 52 \pm 3$ K. However, this Kondo signature disappears when Co atoms are under the molecules (Figure 2a) or on top of them (see Supporting Information). Therefore, Fe is Kondo-screened only when buried under the molecules and Co only as an adatom. The disappearance of the Kondo effect upon formation of metal−organic complexes was reported also for Co bound to TCNE molecules on Cu_2N.[35]

To rationalize our findings, we performed DFT calculations employing the generalized gradient approximation with a mean-field Hubbard correction (GGA+U, with $U = 4$ eV)[36] as implemented in the Quantum-ESPRESSO package.[37] To take into account the van der Waals interaction between molecule and substrate, we included the semiempirical long-range dispersion correction proposed by Grimme.[38,39] The considered slab model consisted of a 6×6 supercell of three layers of Cu(111) with a NC-Ph_3-CN molecule attached to two Cu adatoms with an Fe or Co atom located below the central phenyl ring (see inset in Figure 3a). After relaxation, both

DOI: 10.1021/acsnano.6b07431
ACS Nano 2017, 11, 2675−2681

transition metal adatoms are located in a bridge position of the Cu(111) substrate at ≈1.6 Å above the surface. The central ring of the NC-Ph_3-CN molecule is located at ≈3.1 Å above the substrate, and the molecule is slightly tilted.

The GGA+U calculations predict an atomic magnetic moment of 2.1 and 0.6 μ_B for the buried Fe and Co atoms, respectively. The orbital moments are strongly quenched, indicating that the calculated magnetic moments have mainly spin character. This implies that the Fe atom is in a S = 1 ground state. Table 1 shows the Löwdin spin-up and spin-down

Table 1. Löwdin Populations of the s and d Atomic Orbitals for Fe and Co Atoms Adsorbed under NC-Ph_3-CN on Cu(111)

	s	d_{z^2}	d_{xz}	d_{yz}	$d_{x^2-y^2}$	d_{xy}
Fe spin-up	0.31	0.97	0.92	0.92	0.90	0.89
Fe spin-down	0.28	0.93	0.18	0.20	0.50	0.74
Co spin-up	0.30	0.97	0.87	0.88	0.86	0.85
Co spin-down	0.30	0.95	0.68	0.60	0.80	0.80

occupations[40] of the s and d orbitals for the buried Fe and Co atoms. The x and y coordinates are parallel and perpendicular, respectively, to the long molecular axis in the surface plane. Only orbitals that are partially filled and polarized can lead to a Kondo effect, that is, to screening of the unpaired spin by the conduction electrons, and the resonance is expected to be the most intense for orbitals with only one spin state occupied.[41] The values in Table 1 show that the d orbitals of Co are all almost completely filled, which explains the absence of a Kondo effect for this system. In the case of Fe, on the other hand, the diagonal orbitals d_{xz} and d_{yz} are both nearly singly occupied and fully polarized and can thus yield a Kondo effect. Owing to hybridization, the actual wave functions of the system cannot have a pure atomic character, thus explaining the small spin polarization of the $d_{x^2-y^2}$ and d_{xy} planar orbitals.

In order to establish a connection of the Fe d orbitals with the spatial variation detected in STS, we show in Figure 3a the spin-resolved projected density of states (PDOS) projected onto the Fe and the molecule states, calculated for the slab described above and shown in the inset. The PDOS projected onto the Cu(111) states is omitted for clarity. From Fe 3d orbital-resolved PDOS, we deduce that the states derived from the Fe d_{yz} (labeled A and A′) and d_{xz} (B and B′) orbitals have most of their weight in the energy regions identified by the cyan boxes for majority and minority spins. However, owing to hybridization with the substrate states, they are spread over several electronvolts and the corresponding spatial charge distribution is blurred.

A clearer picture can be obtained from GGA+U calculations for a free-standing NC-Ph_3-CN molecule with an Fe atom attached to the central phenyl ring (see Figure 3b). The PDOS calculated for the free-standing and the surface-supported system presents similarities as, for example, the features of the states corresponding to the planar (star) and d_{z^2} (dot) Fe orbitals. States A (A′) and B (B′), originating mainly from the Fe d_{yz} and d_{xz} orbitals, respectively, are now clearly identified in the PDOS. The d orbital occupations are similar for the two systems (see Tables 1 and 2), indicating that the occupations mostly result from the interaction with the molecule and the Cu(111) substrate plays a minor role. From these observations, we deduce that, for the identification of the atomic orbitals, the free-standing Fe-molecule system is a simplified but appropriate

Table 2. Löwdin Populations of the s and d Atomic Orbitals for the Free-Standing Fe-Molecule System

	s	d_{z^2}	d_{xz}	d_{yz}	$d_{x^2-y^2}$	d_{xy}
Fe spin-up	0.08	0.98	0.97	0.98	0.86	0.86
Fe spin-down	0.08	0.96	0.12	0.11	0.59	0.69

representation of the surface-supported one. Therefore, we use it to describe the contribution of each orbital to the spatial charge distribution.

In Figure 3c, we present the isosurface density plots for the free-standing Fe-molecule system corresponding to states A, B and A′, B′. By inspecting the PDOS in Figure 3b and the isosurface density plots, we conclude that A and A′ are almost pure Fe states, with little or no hybridization with the molecule and extending perpendicularly to the molecular axis, whereas B and B′ have a higher degree of hybridization and are delocalized on the molecular axis. The asymmetry of the resulting hybridized orbitals reflects the spatial dependence observed in STS measurements. Thus, the observed Kondo effect arises from the presence of two screening channels, A and B, one originating mainly from the Fe atomic d_{yz} orbital and the other from the d_{xz} one.

To confirm this interpretation, we estimate the Kondo temperature expected for the states derived from these two d orbitals by using[4]

$$\Gamma = k_B T_K \simeq \sqrt{2\Delta\frac{U}{\pi}}\exp\left[-\frac{\pi}{2\Delta}\left(\left|\frac{1}{\epsilon}\right| + \left|\frac{1}{\epsilon + U}\right|\right)^{-1}\right] \quad (2)$$

where the level binding energy, ϵ, the Coulomb repulsion energy, U, and the hybridization energy between the level and continuum of states in the metal substrate, Δ, appear as parameters. Δ is required to be small with respect to $|\epsilon|$.[4] Qualitatively, state B, being closer to E_F than state A, is expected to yield a higher T_K for a given value of Δ.[4] Considering our results for the free-standing Fe-molecule system, the energies of states A and B are $\epsilon_A = -1.0$ eV and $\epsilon_B = -0.9$ eV. The Coulomb repulsion energy corresponds to the difference between the energy of the occupied and the unoccupied states, U_A = 2.6 eV and U_B = 2.2 eV. We use a typical value of the hybridization energy $\Delta \approx 0.2$ eV,[42] yielding $T_{K,A}$ = 68 K and $T_{K,B}$ = 116 K. These values are in agreement with the experimental Kondo temperatures deduced from the dI/dV spectra, supporting our interpretation of the presence of two distinct Kondo channels, associated with the states derived from d_{yz} (A and A′) and from d_{xz} (B and B′).

It is interesting to note that Fe atoms buried by the molecules have S = 1 with two singly occupied orbitals, as Co atoms on Cu(111).[43] However, in the case of Co/Cu(111), the two orbitals are degenerate, resulting in a single value for T_K.

To investigate the degree of screening of both Kondo channels, we performed X-ray absorption spectroscopy (XAS) and XMCD measurements at the EPFL/PSI X-Treme beamline at the Swiss Light Source.[44] Since the Fe deposition temperature controls the Fe abundance in the three adsorption sites on the (NC-Ph_3-CN)$_3Cu_2$/Cu(111) surface, we can produce samples with the Fe adatoms predominantly adsorbed on the substrate (sample A, T_{dep} = 3 K) and samples where they are mostly below the molecules (sample B, T_{dep} = 40 K). Figure 4a,b compares XAS and XMCD recorded at the Fe $L_{2,3}$ absorption edges of two such samples. As expected, the spectra

DOI: 10.1021/acsnano.6b07431
ACS Nano 2017, 11, 2675−2681

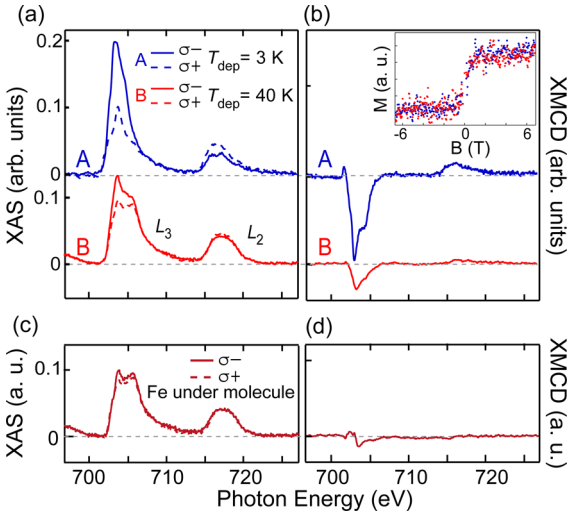

Figure 4. (a) Fe $L_{2,3}$ XAS for samples A and B (B = 6.8 T, T = 2.5 K, Θ = (7 ± 1) × 10^{-3} ML). (b) XMCD of spectra in (a). Inset: Magnetization curves of samples A and B. Curves are scaled to the same saturation value. (c) XAS signal resulting from the subtraction of the contribution of residual Fe atoms on Cu(111) from spectra of sample B and (d) corresponding XMCD. All spectra are normalized to the XAS area.

of sample A are very similar to those measured for Fe atoms on Cu(111).[45] In contrast, the XAS spectra of sample B show a broader L_3 absorption peak and a strongly reduced XMCD signal. As the shapes of the magnetization curves of samples A and B are identical (see inset in Figure 4b), implying an equal response to the external magnetic field, we can conclude that most of the remaining magnetic signal of sample B originates from residual Fe atoms on Cu(111). This is further corroborated by the observation that depositing additional Fe at 3 K results in an increase of the XAS and XMCD intensities, with both spectral shapes approaching the ones measured on the sample with all of the Fe deposited at 3 K (see Supporting Information).

To reveal the signature of the Fe atoms adsorbed under molecules, we removed the contribution of the residual Fe atoms adsorbed on Cu(111). To estimate their amount, we subtracted from the XAS spectrum of sample B in Figure 4a the one Fe on bare Cu(111),[45] rescaled such that the difference does not become negative at any energy (see Supporting Information). With this method, we estimate the residual Fe atoms on the Cu surface to be 20 ± 3% of the total Fe coverage. The resulting XAS and XMCD signals are shown in Figure 4c,d. Applying sum rules to these spectra, using the number of holes n_h = 2.85 found by the DFT calculations, we obtain a spin magnetic moment of only 0.15 ± 0.1 μ_B. A nonscreened S = 1 state would result in a magnetic moment of ≈1.9 μ_B at T = 2.5 K, as estimated using the Brillouin function. Therefore, the magnetic moment of the buried Fe atoms is to a very good approximation entirely Kondo-screened.

Ideally, by performing temperature-dependent measurements, successive suppression of the screening channels should be observed with increasing temperature: the system is expected to turn first into an underscreened impurity, and then the magnetic moment associated with both orbitals is expected to be recovered. However, since XMCD measures the magnetic moment projected onto the photon beam direction, which is parallel to the external magnetic field, the gain of magnetic moment due to the disruption of the Kondo state is in competition with the temperature-induced decrease of its projection expected for a paramagnetic system. Measurements at 40 K show that the projected spin magnetic moment of the Fe atoms adsorbed under molecules does not change significantly with respect to the value obtained at 3 K (see Supporting Information). This observation indicates that the absolute value of the magnetic moment must have increased, thus confirming that the screening effect is partially lost at 40 K.

CONCLUSIONS

In conclusion, we have shown that the combination of transition metal atoms and organic molecules can suppress the Kondo effect in the case of Co, while inducing it for Fe, leading to a regular array of Kondo impurities. In addition, these impurities have two distinct screening channels that originate from nondegenerate orbitals and give rise to a Kondo effect with different signatures in the directions parallel and perpendicular to the molecular axis. The effective screening of the spin in both channels is finally demonstrated through XAS and XMCD measurements.

METHODS

Sample Preparation. The Cu(111) substrate was prepared by Ar^+ sputtering (2 μA/cm^2, 800 V, 20 min) and annealing (800 K, 20 min) cycles. NC-Ph_3-CN molecules were evaporated from a molecular effusion cell at 418 K onto the Cu(111) substrate at 300 K. The obtained (NC-Ph_3-CN)$_3$$Cu_2$ honeycomb network has a period of 3.51 nm.[25]

Fe and Co were evaporated from an e-beam evaporator, while the sample was placed in the STM. One monolayer of Fe or Co is defined as one atom per Cu(111) unit cell.

STM. STM and STS experiments were performed with a 5 K ultrahigh vacuum STM[46] using W tips. Indicated bias voltages, V_b, refer to the sample.

In all STS measurements, the voltage modulation refers to peak-to-peak values. All spectra are averaged over several measurements, and a reference spectrum acquired on the substrate has been subtracted. The differential conductance map is extracted from a grid of 32 × 16 dI/dV spectra.

DFT. The DFT calculations were performed within the density functional theory framework employing the generalized gradient approximation (GGA) with a mean-field Hubbard correction (GGA +U)[36] as implemented in the Quantum-ESPRESSO package.[37] We used ultrasoft pseudopotentials, a planewave cutoff of 30 Ry, and a Hubbard parameter U of 4 eV for the Fe and Co d orbitals. We checked the convergence with respect to the cutoff and tested different values of U (namely, U = 2 and 3 eV), which give very similar results. The structure was fully relaxed using a 2 × 2 k-point mesh until all residual forces were below 10^{-3} Ha/a_0. The density of states and magnetic properties were then computed self-consistently on a 4 × 4 k-point mesh. The atomic magnetic moment and the Löwdin population of the Fe and Co orbitals were obtained by projecting the Kohn−Sham wave functions onto a set of localized atomic orbitals.

XMCD. We recorded the $L_{2,3}$ absorption edges of Fe in the total electron yield mode. The Cu(111) preparation and the molecule deposition were performed in the preparation chamber of X-Treme,[44] and Fe was deposited after the sample had been transferred *in situ* into the cryostat. Molecule and Fe coverages were calibrated by cross-correlating XAS spectra with *in situ* STM measurements. The STM was also employed to check the quality of the metal−organic honeycomb structure. The magnetization curves were obtained as the amplitude of the L_3 XMCD peak intensity at 703.5 eV divided by the pre-edge signal at 701.5 eV. The spectra are normalized to the XAS area.

DOI: 10.1021/acsnano.6b07431
ACS Nano 2017, 11, 2675−2681

ASSOCIATED CONTENT

Supporting Information

The Supporting Information is available free of charge on the ACS Publications website at DOI: 10.1021/acsnano.6b07431.

STM and STS results of (i) manipulation of Fe adatoms, (ii) Fe atoms buried by NC-Ph_5-CN molecules in (NC-Ph_5-CN)$_3$$Cu_2$/Cu(111), (iii) d$I$/d$V$ spectroscopy on related systems, (iv) fitting parameters of dI/dV spectra reported in the main text; XAS and XMCD results of (i) dependence on deposition temperature, (ii) subtraction of signal due to residual Fe/Cu, and (iii) temperature-dependent measurements (PDF)

AUTHOR INFORMATION

Corresponding Author

*E-mail: harald.brune@epfl.ch.

ORCID

Marina Pivetta: 0000-0001-5330-8648

Luca Gragnaniello: 0000-0003-1150-3941

Harald Brune: 0000-0003-4459-3111

Notes

The authors declare no competing financial interest.

ACKNOWLEDGMENTS

We acknowledge M. Ruben, S. Klyatskaya, and J.V. Barth for providing us with the organic molecules, as well as J. Dreiser and C. Piamonteze for their assistance with the experiments at X-Treme. We thank the Swiss National Science Foundation for financial support (Grant Nos. 200020_140479 and 200020_157081). G.A. and O.V.Y. acknowledge the Swiss National Science Foundation (Grant No. PP00P2_133552) and NCCR-MARVEL. First-principles calculations were performed at the Swiss National Supercomputing Center (CSCS) under project s675.

REFERENCES

(1) Kondo, J. Resistance Minimum in Dilute Magnetic Alloys. *Prog. Theor. Phys.* **1964**, *32*, 37−49.

(2) Madhavan, V.; Chen, W.; Jamneala, T.; Crommie, M. F.; Wingreen, N. S. Tunneling into a Single Magnetic Atom: Spectroscopic Evidence of the Kondo Resonance. *Science* **1998**, *280*, 567−569.

(3) Manoharan, H. C.; Lutz, C. P.; Eigler, D. M. Quantum Mirages Formed by Coherent Projection of Electronic Structure. *Nature* **2000**, *403*, 512−515.

(4) Ternes, M.; Heinrich, A. J.; Schneider, W.-D. Spectroscopic Manifestation of the Kondo Effect on Single Adatoms. *J. Phys.: Condens. Matter* **2009**, *21*, 053001.

(5) Goldhaber-Gordon, D.; Shtrikman, H.; Mahalu, D.; Abusch-Magder, D.; Meirav, U.; Kastner, M. A. Kondo Effect in a Single-Electron Transistor. *Nature* **1998**, *391*, 156−159.

(6) Cronenwett, S. M.; Oosterkamp, T. H.; Kouwenhoven, L. P. A Tunable Kondo Effect in Quantum Dots. *Science* **1998**, *281*, 540−544.

(7) Bogani, L.; Wernsdorfer, W. Molecular Spintronics Using Single-Molecule Magnets. *Nat. Mater.* **2008**, *7*, 179−186.

(8) Scott, G. D.; Natelson, D. Kondo Resonances in Molecular Devices. *ACS Nano* **2010**, *4*, 3560−3579.

(9) Robles, R.; Lorente, N.; Isshiki, H.; Liu, J.; Katoh, K.; Breedlove, B. K.; Yamashita, M.; Komeda, T. Spin Doping of Individual Molecules by Using Single-Atom Manipulation. *Nano Lett.* **2012**, *12*, 3609−3612.

(10) Liu, J.; Isshiki, H.; Katoh, K.; Morita, T.; Breedlove, B. K.; Yamashita, M.; Komeda, T. First Observation of a Kondo Resonance for a Stable Neutral Pure Organic Radical, 1,3,5-Triphenyl-6-oxoverdazyl, Adsorbed on the Au(111) Surface. *J. Am. Chem. Soc.* **2013**, *135*, 651−658.

(11) Kim, H.; Chang, Y. H.; Lee, S.-H.; Kim, Y.-H.; Kahng, S.-J. Switching and Sensing Spin States of Co-Porphyrin in Bimolecular Reactions on Au(111) Using Scanning Tunneling Microscopy. *ACS Nano* **2013**, *7*, 9312−9317.

(12) Liu, L.; Yang, K.; Jiang, Y.; Song, B.; Xiao, W.; Li, L.; Zhou, H.; Wang, Y.; Du, S.; Ouyang, M.; Hofer, W. A.; Castro Neto, A. H.; Gao, H.-J. Reversible Single Spin Control of Individual Magnetic Molecule by Hydrogen Atom Adsorption. *Sci. Rep.* **2013**, *3*, 1210.

(13) Iancu, V.; Braun, K.-F.; Schouteden, K.; Van Haesendonck, C. Inducing Magnetism in Pure Organic Molecules by Single Magnetic Atom Doping. *Phys. Rev. Lett.* **2014**, *113*, 106102.

(14) Zhao, A.; Li, Q.; Chen, L.; Xiang, H.; Wang, W.; Pan, S.; Wang, B.; Xiao, X.; Yang, J.; Hou, J. G.; Zhu, Q. Controlling the Kondo Effect of an Adsorbed Magnetic Ion Through Its Chemical Bonding. *Science* **2005**, *309*, 1542−1544.

(15) Fernández-Torrente, I.; Franke, K. J.; Pascual, J. I. Vibrational Kondo Effect in Pure Organic Charge-Transfer Assemblies. *Phys. Rev. Lett.* **2008**, *101*, 217203.

(16) Zhang, Q.; Kuang, G.; Pang, R.; Shi, X.; Lin, N. Switching Molecular Kondo Effect *via* Supramolecular Interaction. *ACS Nano* **2015**, *9*, 12521−12528.

(17) Choi, T.; Bedwani, S.; Rochefort, A.; Chen, C.-Y.; Epstein, A. J.; Gupta, J. A. A Single Molecule Kondo Switch: Multistability of Tetracyanoethylene on Cu(111). *Nano Lett.* **2010**, *10*, 4175−4180.

(18) Komeda, T.; Isshiki, H.; Liu, J.; Zhang, Y.-F.; Lorente, N.; Katoh, K.; Breedlove, B. K.; Yamashita, M. Observation and Electric Current Control of a Local Spin in a Single-Molecule Magnet. *Nat. Commun.* **2011**, *2*, 217.

(19) Karan, S.; Li, N.; Zhang, Y.; He, Y.; Hong, I.-P.; Song, H.; Lü, J.-T.; Wang, Y.; Peng, L.; Wu, K.; Michelitsch, G. S.; Maurer, R. J.; Diller, K.; Reuter, K.; Weismann, A.; Berndt, R. Spin Manipulation by Creation of Single-Molecule Radical Cations. *Phys. Rev. Lett.* **2016**, *116*, 027201.

(20) Mugarza, A.; Krull, C.; Robles, R.; Stepanow, S.; Ceballos, G.; Gambardella, P. Spin Coupling and Relaxation Inside Molecule-Metal Contacts. *Nat. Commun.* **2011**, *2*, 490.

(21) Franke, K. J.; Schulze, G.; Pascual, J. I. Competition of Superconducting Phenomena and Kondo Screening at the Nanoscale. *Science* **2011**, *332*, 940−944.

(22) Stróżecka, A.; Soriano, M.; Pascual, J. I.; Palacios, J. J. Reversible Change of the Spin State in a Manganese Phthalocyanine by Coordination of CO Molecule. *Phys. Rev. Lett.* **2012**, *109*, 147202.

(23) Wang, W.; Pang, R.; Kuang, G.; Shi, X.; Shang, X.; Liu, P. N.; Lin, N. Intramolecularly Resolved Kondo Resonance of High-Spin Fe(II)-Porphyrin Adsorbed on Au(111). *Phys. Rev. B: Condens. Matter Mater. Phys.* **2015**, *91*, 045440.

(24) Schlickum, U.; Decker, R.; Klappenberger, F.; Zoppellaro, G.; Klyatskaya, S.; Ruben, M.; Silanes, I.; Arnau, A.; Kern, K.; Brune, H.; Barth, J. V. Metal-Organic Honeycomb Nanomeshes with Tunable Cavity Size. *Nano Lett.* **2007**, *7*, 3813−3817.

(25) Pacchioni, G. E.; Pivetta, M.; Brune, H. Competing Interactions in the Self-Assembly of NC-Ph_3-CN Molecules on Cu(111). *J. Phys. Chem. C* **2015**, *119*, 25442−25448.

(26) Pivetta, M.; Pacchioni, G. E.; Schlickum, U.; Barth, J. V.; Brune, H. Formation of Fe Cluster Superlattice in a Metal-Organic Quantum-Box Network. *Phys. Rev. Lett.* **2013**, *110*, 086102.

(27) Zhong, D. Y.; Franke, J.; Blömker, T.; Erker, G.; Chi, L. F.; Fuchs, H. Manipulating Surface Diffusion Ability of Single Molecules by Scanning Tunneling Microscopy. *Nano Lett.* **2009**, *9*, 132−136.

(28) Klappenberger, F.; Kühne, D.; Marschall, M.; Neppl, S.; Krenner, W.; Nefedov, A.; Strunskus, T.; Fink, K.; Wöll, C.; Klyatskaya, S.; Fuhr, O.; Ruben, M.; Barth, J. V. Uniform π-System Alignment in Thin Films of Template-Grown Dicarbonitrile-Oligophenyls. *Adv. Funct. Mater.* **2011**, *21*, 1631−1642.

(29) Wang, S.; Wang, W.; Lin, N. Resolving Band-Structure Evolution and Defect-Induced States of Single Conjugated Oligomers

DOI: 10.1021/acsnano.6b07431
ACS Nano 2017, 11, 2675−2681

by Scanning Tunneling Microscopy and Tight-Binding Calculations. *Phys. Rev. Lett.* **2011**, *106*, 206803.
(30) Fano, U. Effects of Configuration Interaction on Intensities and Phase Shifts. *Phys. Rev.* **1961**, *124*, 1866−1878.
(31) Nagaoka, K.; Jamneala, T.; Grobis, M.; Crommie, M. F. Temperature Dependence of a Single Kondo Impurity. *Phys. Rev. Lett.* **2002**, *88*, 077205.
(32) Otte, A. F.; Ternes, M.; von Bergmann, K.; Loth, S.; Brune, H.; Lutz, C. P.; Hirjibehedin, C. F.; Heinrich, A. J. The Role of Magnetic Anisotropy in the Kondo Effect. *Nat. Phys.* **2008**, *4*, 847−850.
(33) Perera, U. G. E.; Kulik, H. J.; Iancu, V.; Dias da Silva, L. G. G. V.; Ulloa, S. E.; Marzari, N.; Hla, S.-W. Spatially Extended Kondo State in Magnetic Molecules Induced by Interfacial Charge Transfer. *Phys. Rev. Lett.* **2010**, *105*, 106601.
(34) Knorr, N.; Schneider, M. A.; Diekhöner, L.; Wahl, P.; Kern, K. Kondo Effect of Single Co Adatoms on Cu Surfaces. *Phys. Rev. Lett.* **2002**, *88*, 096804.
(35) Choi, T.; Badal, M.; Loth, S.; Yoo, J.-W.; Lutz, C. P.; Heinrich, A. J.; Epstein, A. J.; Stroud, D. G.; Gupta, J. A. Magnetism in Single Metalloorganic Complexes Formed by Atom Manipulation. *Nano Lett.* **2014**, *14*, 1196−1201.
(36) Anisimov, V. I.; Zaanen, J.; Andersen, O. K. Band Theory and Mott Insulators: Hubbard U Instead of Stoner I. *Phys. Rev. B: Condens. Matter Mater. Phys.* **1991**, *44*, 943−954.
(37) Giannozzi, P.; Baroni, S.; Bonini, N.; Calandra, M.; Car, R.; Cavazzoni, C.; Ceresoli, D.; Chiarotti, G. L.; Cococcioni, M.; Dabo, I.; Dal Corso, A.; de Gironcoli, S.; Fabris, S.; Fratesi, G.; Gebauer, R.; Gerstmann, U.; Gougoussis, C.; Kokalj, A.; Lazzeri, M.; Martin-Samos, L.; et al. QUANTUM ESPRESSO: a Modular and Open-Source Software Project for Quantum Simulations of Materials. *J. Phys.: Condens. Matter* **2009**, *21*, 395502.
(38) Grimme, S. Semiempirical GGA-Type Density Functional Constructed with a Long-Range Dispersion Correction. *J. Comput. Chem.* **2006**, *27*, 1787−1799.
(39) Barone, V.; Casarin, M.; Forrer, D.; Pavone, M.; Sambi, M.; Vittadini, A. Role and Effective Treatment of Dispersive Forces in Materials: Polyethylene and Graphite Crystals as Test Cases. *J. Comput. Chem.* **2009**, *30*, 934−939.
(40) Löwdin, P.-O. On the Non-Orthogonality Problem Connected with the Use of Atomic Wave Functions in the Theory of Molecules and Crystals. *J. Chem. Phys.* **1950**, *18*, 365−375.
(41) Kügel, J.; Karolak, M.; Senkpiel, J.; Hsu, P.-J.; Sangiovanni, G.; Bode, M. Relevance of Hybridization and Filling of 3d Orbitals for the Kondo Effect in Transition Metal Phthalocyanines. *Nano Lett.* **2014**, *14*, 3895−3902.
(42) Újsághy, O.; Kroha, J.; Szunyogh, L.; Zawadowski, A. Theory of the Fano Resonance in the STM Tunneling Density of States due to a Single Kondo Impurity. *Phys. Rev. Lett.* **2000**, *85*, 2557−2560.
(43) Baruselli, P. P.; Requist, R.; Smogunov, A.; Fabrizio, M.; Tosatti, E. Co Adatoms on Cu Surfaces: Ballistic Conductance and Kondo Temperature. *Phys. Rev. B: Condens. Matter Mater. Phys.* **2015**, *92*, 045119.
(44) Piamonteze, C.; Flechsig, U.; Rusponi, S.; Dreiser, J.; Heidler, J.; Schmidt, M.; Wetter, R.; Calvi, M.; Schmidt, T.; Pruchova, H.; Krempasky, J.; Quitmann, C.; Brune, H.; Nolting, F. X-Treme Beamline at SLS: X-Ray Magnetic Circular and Linear Dichroism at High Field and Low Temperature. *J. Synchrotron Radiat.* **2012**, *19*, 661−674.
(45) Pacchioni, G. E.; Gragnaniello, L.; Donati, F.; Pivetta, M.; Autès, G.; Yazyev, O. V.; Rusponi, S.; Brune, H. Multiplet Features and Magnetic Properties of Fe on Cu(111): From Single Atoms to Small Clusters. *Phys. Rev. B: Condens. Matter Mater. Phys.* **2015**, *91*, 235426.
(46) Gaisch, R.; Gimzewski, J. K.; Reihl, B.; Schlittler, R. R.; Tschudy, M.; Schneider, W. D. Low-Temperature Ultra-High Vacuum Scanning Tunneling Microscope. *Ultramicroscopy* **1992**, *42*−*44*, 1621−1626.

DOI: 10.1021/acsnano.6b07431
ACS Nano 2017, 11, 2675−2681

Supporting information for:

Two-Orbital Kondo Screening in a Self-Assembled Metal-Organic Complex

Giulia E. Pacchioni, Marina Pivetta, Luca Gragnaniello, Fabio Donati, Gabriel Autès, Oleg V. Yazyev, Stefano Rusponi, and Harald Brune*

Institute of Physics, Ecole Polytechnique Fédérale de Lausanne (EPFL), CH-1015 Lausanne, Switzerland

E-mail: harald.brune@epfl.ch

STM and STS

Manipulation of Fe adatoms

Figure S1 demonstrates that the very bright features observed on STM images (indicated by yellow arrows) are single atoms adsorbed on molecules. Indeed, after repeated imaging, these objects disappear and single atoms, marked by the turquoise dashed circles, are found in close-by cavities.

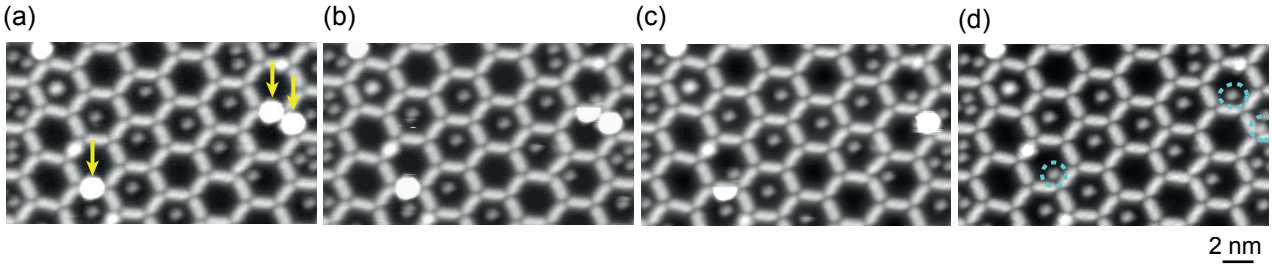

Figure S1: Consecutive images showing the successive descent of Fe atoms from ontop of the molecules in the (NC-Ph_3-CN)$_3Cu_2$/Cu(111) honeycomb network down to the substrate. Fe deposition: $\Theta = (6 \pm 1) \times 10^{-3}$ ML, $T_{\mathrm{dep}} = 10 \pm 2$ K. ($V_{\mathrm{t}} = -300$ mV, $I_{\mathrm{t}} = 50$ pA, $T_{\mathrm{STM}} = 5$ K).

Fe on (NC-Ph_5-CN)$_3Cu_2$/Cu(111)

Figure S2 shows results for Fe deposition on honeycomb networks built with a longer polyphenyl molecules, namely, (NC-Ph_5-CN)$_3Cu_2$/Cu(111).[S1] Deposition between 20 and 50 K leads to diffusion of the Fe atoms under the molecules. Different to the result obtained with NC-Ph_3-CN molecules, in this case small clusters are often formed, visible as the brightest spots in the STM image in Fig. S2(a). Buried single Fe atoms appear as smaller, dimmer features, as the one encircled. Figure S2(b) shows an STM image and the corresponding dI/dV map at E_{F}. The images show several NC-Ph_5-CN molecules, some of them with an Fe atom below a phenyl ring (white arrows). The bottom-left molecule also hosts a bigger object, identified as an Fe cluster (green arrow). For each buried Fe atom, the dI/dV map at E_{F} shows a large bright spot on one side of the molecular axis and a less bright, smaller one on the opposite side; a depression is observed in correspondence of the molecular axis. Notice that these spectroscopic features are absent for the buried Fe cluster (green arrow).

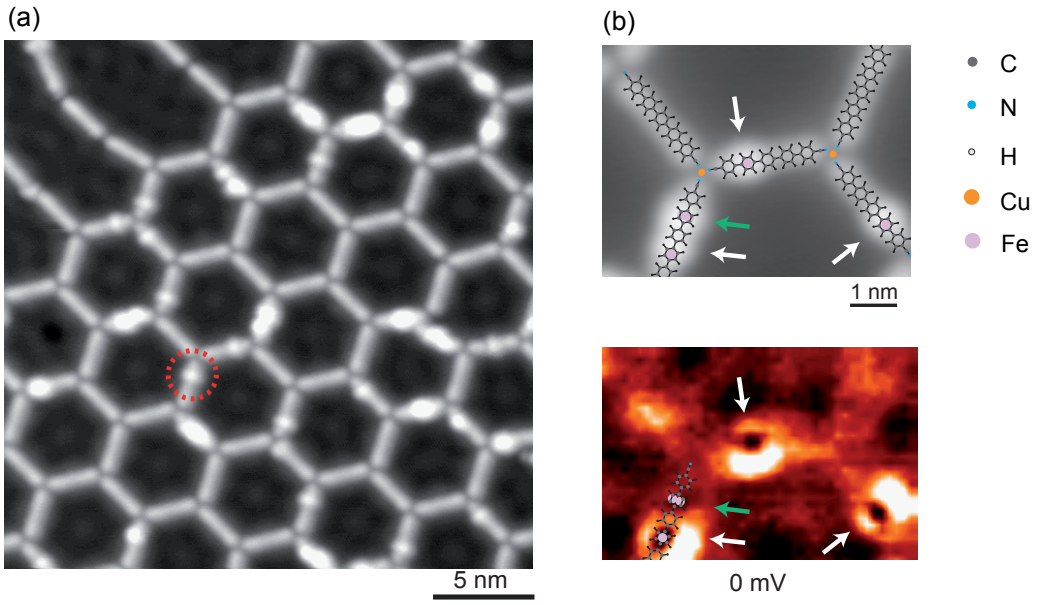

Figure S2: (a) STM image of the (NC-Ph$_5$-CN)$_3$Cu$_2$ honeycomb network on Cu(111) for $\Theta = (6 \pm 1) \times 10^{-3}$ ML of Fe deposited at $T_{\mathrm{dep}} = 32$ K. The red circle indicates a buried Fe atom ($V_{\mathrm{t}} = -50$ mV, $I_{\mathrm{t}} = 300$ pA, $T_{\mathrm{STM}} = 5$ K). (b) Smaller scale STM image, white arrows indicate buried Fe atoms, the green arrow points at an Fe cluster ($V_{\mathrm{t}} = -300$ mV, $I_{\mathrm{t}} = 800$ pA, $T_{\mathrm{STM}} = 5$ K); corresponding dI/dV map at E_{F} ($V_{\mathrm{mod}} = 2$ mV at 523 Hz).

STS spectroscopy on related systems

Figure S3(a) shows the dI/dV spectra acquired on Co atoms adsorbed on NC-Ph$_3$-CN molecules. In Fig. S3(b) spectra measured on Fe atoms on NC-Ph$_3$-CN and on the pristine molecules are presented. None of the spectra show Kondo features.

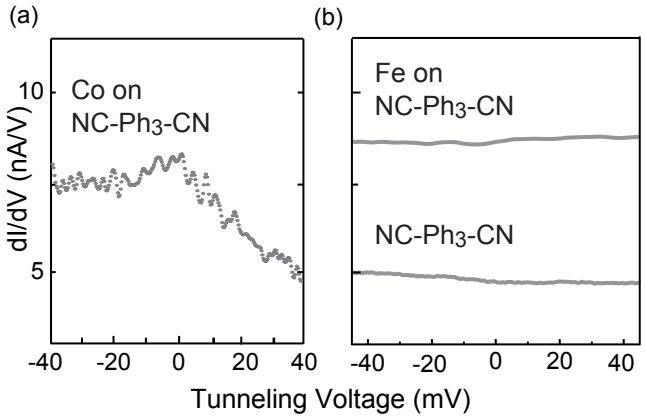

Figure S3: dI/dV spectra acquired on the indicated systems on Cu(111): (a) Co on NC-Ph$_3$-CN; (b) bare NC-Ph$_3$-CN and Fe on NC-Ph$_3$-CN; spectra are offset for clarity. Setpoint: $V_{\mathrm{t}} = -50$ mV, $I_{\mathrm{t}} = 300$ pA, $V_{\mathrm{mod}} = 2$ mV peat-to-peak at 523 Hz.

Fitting parameters

Values of Γ_0 and q obtained from the fits in Fig. 2(a) in the main text (using $\alpha = 5$[S2,S3]):

Fe under NC-Ph_3-CN	main peak:	$\Gamma_0 = 5.4 \pm 0.3$ meV, $q = 10$
	less intense peak:	$\Gamma_0 = 5.3 \pm 0.2$ meV, $q = 3$
	dip:	$\Gamma_0 = 9.8 \pm 0.5$ meV, $q = -0.6$
Co/Cu(111):		$\Gamma_0 = 4.5 \pm 0.3$ meV and $q = 0.4$

XAS and XMCD

Dependence on the deposition temperature

Most of the Fe atoms on sample B in the main paper ($T_{\mathrm{dep}} = 40$ K) are buried under the molecules. This sample shows a much weaker XMCD signal (red in Fig. 4 and Fig. S4) than sample A ($T_{\mathrm{dep}} = 3$ K, blue in Fig. 4). To explain the origin of this difference, we have added Fe atoms at 3 K on sample B (Fig. S4, green). At this deposition temperature, Fe atoms come to rest on their impact site which is predominantly bare Cu(111). This results in an increase of the XAS and XMCD intensities, see Figs. S4(a) and (b), with both spectral shapes approaching the ones measured on the sample with all of the Fe deposited at 3 K.

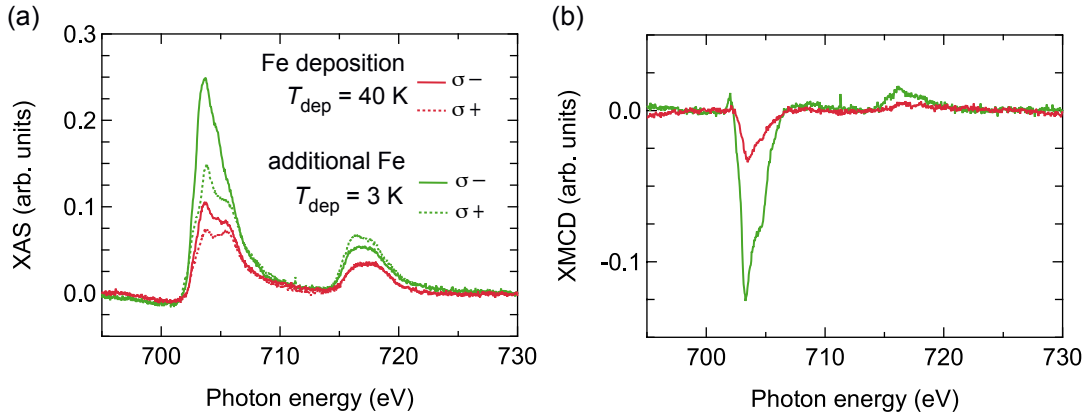

Figure S4: XAS (a) and corresponding XMCD (b) spectra of a sample on which Fe was evaporated at 40 K (red, sample B), $\Theta = (7 \pm 1) \times 10^{-3}$ ML and further Fe was added at 3 K (green), final coverage $\Theta = (1.4 \pm 0.2) \times 10^{-2}$ ML. The spectra are normalized to the XAS area for the first deposition.

Subtraction of the signal of residual Fe/Cu(111)

We estimate for sample B the relative amount of Fe present on bare Cu(111) and buried under the molecules by subtracting the spectrum of Fe on bare Cu(111)[S4] from the XAS spectrum of sample B. The amount of Fe on bare Cu(111) is then given by the scaling factor needed for the Fe/Cu(111) spectrum such that the difference does not become negative for any energy, see Fig. S5(a). The green circle highlights the part of the spectra that would result in a negative XAS in the difference spectrum if the signal coming from Fe on bare Cu(111) was overestimated. We find that the amount of Fe adsorbed on the bare Cu in sample B is $20 \pm 3\,\%$. The result of the subtraction is shown in Fig. S5(b). In Fig. 4 in the main text we report the two polarizations as well as the XMCD signal.

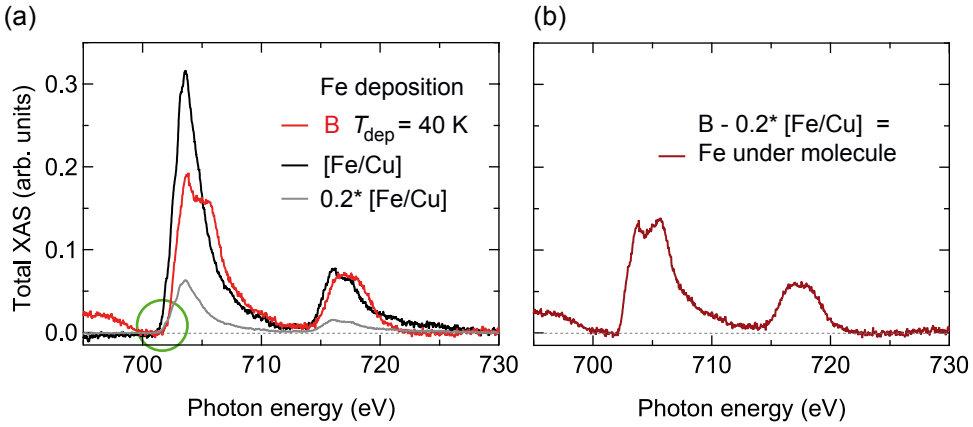

Figure S5: (a) Total XAS of sample B in the main text (red) and total XAS of Fe atoms on Cu(111) (black). Gray: spectrum of Fe on Cu rescaled by a factor 0.2. Fe coverage is $\Theta = (7 \pm 1) \times 10^{-3}$ ML for both samples. The spectra are normalized to the XAS area. (b) Result of the difference to extract the total XAS of Fe atoms buried by molecules.

Temperature-dependent measurements

Figure S6(a) shows XAS spectra of the Fe atoms under molecules obtained with the procedure described above from spectra acquired at 40 K and at 3 K. For the 40 K data, the procedure is applied keeping for the Fe/Cu an unmodified XAS value and reducing the XMCD by a factor of 3.7. This factor corresponds to the ratio of the Fe moment at 3 K and 40 K as derived from moments and anisotropy values given in Ref.[S4] For this sample we

deduce a spin magnetic moment of 0.3 ± 0.1 μ_B at 3 K and of 0.4 ± 0.1 μ_B at 40 K.

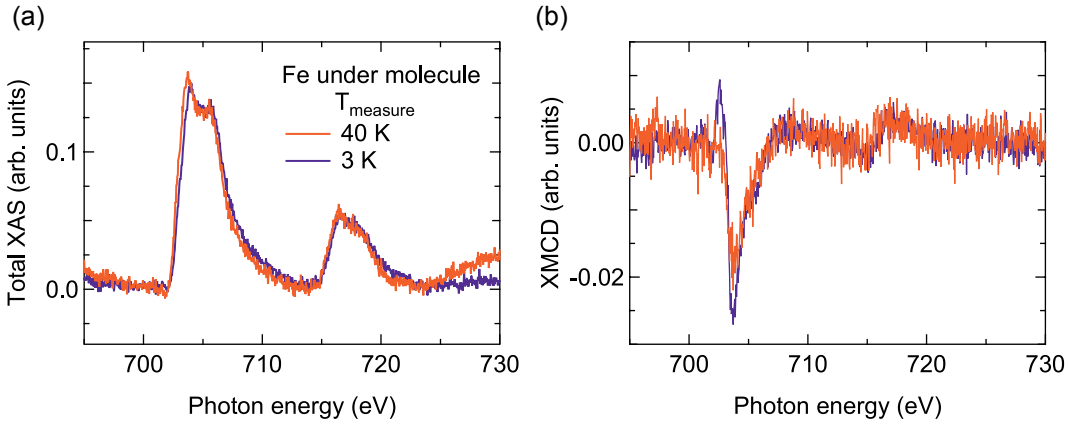

Figure S6: (a) Total XAS and (b) XMCD of Fe under molecules for the same sample measured at 40 K and 3 K. Fe coverage is $\Theta = (7 \pm 1) \times 10^{-3}$ ML. The spectra are normalized to the XAS area.

References

(S1) Pivetta, M.; Pacchioni, G. E.; Schlickum, U.; Barth, J. V.; Brune, H. Formation of Fe Cluster Superlattice in a Metal-Organic Quantum-Box Network. *Phys. Rev. Lett.* **2013**, *110*, 086102.

(S2) Nagaoka, K.; Jamneala, T.; Grobis, M.; Crommie, M. F. Temperature Dependence of a Single Kondo Impurity. *Phys. Rev. Lett.* **2002**, *88*, 077205.

(S3) Otte, A. F.; Ternes, M.; von Bergmann, K.; Loth, S.; Brune, H.; Lutz, C. P.; Hirjibehedin, C. F.; Heinrich, A. J. The Role of Magnetic Anisotropy in the Kondo Effect. *Nat. Phys.* **2008**, *4*, 847.

(S4) Pacchioni, G. E.; Gragnaniello, L.; Donati, F.; Pivetta, M.; Autès, G.; Yazyev, O. V.; Rusponi, S.; Brune, H. Multiplet Features and Magnetic Properties of Fe on Cu(111): From Single Atoms to Small Clusters. *Phys. Rev. B* **2015**, *91*, 235426.